preprint; submitted to Physical Review B in December 2002

The Energetics of Li Off-Centering in $K_{1-x}Li_xTaO_3$; First Principles Calculations

S. A. Prosandeev[1,2], E. Cockayne[1], and B. P. Burton[1]

[1] *Ceramics Division, Materials Science and Engineering Laboratory, National Institute of Standards and Technology, Gaithersburg, Maryland 20899-8520*

[2] *Physics Department, Rostov State University, 5 Zorge St., 344090 Rostov on Don, Russia*

$K_{1-x}Li_xTaO_3$ (KLT) solid solutions exhibit a variety of interesting physical phenomena related to large local displacements of Li-ions from ideal perovskite A-site positions. First-principles calculations for KLT supercells were used to investigate these phenomena. Lattice dynamics calculations show that KLT has a Li off-centering instability. The energetics of Li-displacements for isolated Li-ions and for Li-Li pairs up to 4th neighbors were calculated. The interaction between nearest neighbor Li-ions strongly favors ferroelectric alignment along their mutual axis. Such Li-Li pairs can be considered as "seeds" for polar nanoclusters in KLT. Electrostriction, local oxygen relaxation, coupling to the KT soft-mode, and an interaction with neighboring Li-ions all enhance the polarization arising from Li off-centering. Calculated hopping barriers for isolated Li-ions and for nearest neighbor Li-Li pairs are in good agreement with Arrhenius fits to experimental dielectric data.

PACS numbers:

I. INTRODUCTION

Potassium tantalate, $KTaO_3$ (KT), is a cubic perovskite with a quantum paraelectric ground state.[1] In $K_{1-x}Li_xTaO_3$ (KLT) solid solutions, Li-ions substitute for K on perovskite A-sites. Li-ions are smaller than K, and displace from ideal A-sites by about 1.26 Å[2] along cubic [001]-type vectors. Displacements of Li-ions from ideal centrosymmetric positions generates strong local dipole moments [Li-dipole(s)] which couple electrostatically to the KT polar soft-mode. Near neighbor (nn) Li-dipoles can also interact to form polar nanoclusters (PNC); i.e. multiatom regions in which the local polarization direction is strongly correlated. The complex nature of ferroelectric (FE) ordering in KLT derives from a combination of interactions between Li-dipoles, the soft-mode, and PNC.

In the composition range $0 < x < 0.02$, KLT is a quantum paraelectric, but for $0.02 < x < 0.06$, both FE and dipole-glass characteristics are observed.[3–5] In the temperature (T) interval $0 < T \lesssim 100$ K, the dielectric permittivity, $\varepsilon(T)$, has a peak, and second harmonic generation exhibits an abrupt increase, with hysteresis.[6,7] The existence of randomly distributed and randomly poled PNC was established from dielectric measurements, birefringence and NMR.[3,5,8,9] According to Ref. [7], neighboring PNC may touch, but PNC-coarsening is prevented by random long-range PNC-PNC interactions. Absent an applied field, a glassy phase is observed.[5], however, a sufficient applied field will induce FE long-range order (LRO).[3,5,6] For $0.06 \lesssim x < 0.15$, KLT undergoes a FE phase transition at T $\gtrsim$ 100K, even in the absence of an applied field. At larger Li-concentrations a perovskite structure phase is no longer stable.

Dielectric measurements on KLT with $0 < x < 0.02$ exhibit only one relaxational peak in $\varepsilon(T)$, while at $x \sim 0.04$, two peaks are observed, and they are associated with two relaxational processes (fast and slow).[8,10–12] Temperature variations of both relaxation processes follow Arrhenius laws; $\tau \sim Ce^{-U/kT}$. The fast process activation energy is $U \approx 1000$ K (86 meV), and the slow process, at $0.02 < x < 0.06$, has been reported as ~ 2100 K,[13] ~ 2400 K[11] and ~ 2800 K.[12]

The 1000 K activation energy is believed to be the barrier for an isolated Li-ion to hop from one [001]-type position to another separated by a 90° angle. NMR data support this hypothesis.[2] The nature of the slow process with $2100 \lesssim U \lesssim 2800$ K[11–13] is not well understood. On the basis of acoustic measurements it was hypothesized[8,10] that it might be associated with Li-Li nearest-neighbor (nn) pairs that undergo correlated 180° reorientations (*e.g.* $z - z \rightleftharpoons \overline{z} - \overline{z}$ relaxation for nn separated by $a_0\hat{z}$ where a_0 is the lattice parameter of the primitive unit cell, and $\hat{z}$ is a unit vector in the $[0, 0, z]$ direction).

The energy spectrum and kinetics of PNC reorientation is a general problem for FE systems that exhibit both relaxor and soft-mode behavior (c.f.[14]). KLT is a relatively simple model system for such phenomena, because isolated Li-ions in KLT solutions can be regarded as randomly distributed sources of 6-state Potts-like dipole fields.[15–17] Previous modeling includes: Semi-empirical shell model calculations[18]; Intermediate neglect of the differential overlap (INDO) calculations[19,20]; Full potential linear muffin-tin orbital (FPLMTO) calculations.[20,21] (without ionic relaxations). All these studies yielded potential barriers for 90° Li-hopping that were significantly lower than those deduced from experimental fits.

KLT solutions with $0.016 < x < 0.05$ exhibit a large photocurrent below 80K.[22–24] No photocurrent has been

observed in pure KT, nor in solid solutions of KT with Nb. This photocurrent is usually thought to be associated with O-hole centers near Li-occupied A-sites[22]. Recent INDO calculations[20] confirmed that shallow states appear in the forbidden gap due to displacements of oxygen ions that are nn of Li.

First-principles (FP) computations allow determination of the electronic structure and energetics as a functions of ionic coordinates, and thus provide a sound basis for understanding and quantitatively modeling of KLT.

In this work, FP density functional theory (DFT) methods were used to calculate the energetics of Li off-centering for isolated Li-ions and for Li-Li pairs up to fourth neighbors in KLT supercells. The energetics of 90° hopping of isolated Li-ions and 180° hopping of Li-Li nn-pairs were calculated. The lattice dynamics of KLT were studied, demonstrating correlated motions of Li and the surrounding ions (particularly nn O). Total polarization from Li off-centering, and individual contributions from different ions were quantified. Electronic band structures were calculated to investigate shallow electronic states that may promote photocurrent.

II. METHODS

All DFT calculations were done with the Vienna *ab initio* simulation package (VASP)[25,26]. A plane wave basis set for electronic wavefunctions, and ultrasoft pseudopotentials were used,[27] in the local density approximation (LDA) for exchange and correlation energies. VASP computes interatomic forces and total energies for crystals, and allows either global or constrained relaxations of internal coordinates and/or lattice parameters. Frozen-phonon methods were used to obtain force constants for computing lattice dynamics. Berry phase analyses, as implemented in VASP by M. Marsman, were used to calculate dynamical charges.

Investigating the effects of Li-ions in KLT with low Li concentration requires large supercells, *e.g.* (Figure 1): (a) KT40, a 40 atom supercell of pure $KTaO_3$; (b) KLT40, a 40 atom supercell with basis vectors [002], [020] and [200] (units of a_0, $x = 0.125$); (c) KLT80a an 80 atom supercell with basis vectors [220], [202], and [022] and $x = 0.0625$; (d) KLT80b, same as KLT80a but with two Li per supercell, $x = 0.125$, separated by $a_0\hat{z}$; (e,f,g) KLT80c, KLT80d, KLT80e, same as KLT80b, but with 2 Li separated by $a_0(\hat{x}+\hat{y})$, $a_0(\hat{x}+\hat{y}+\hat{z})$ and $2a_0\hat{z}$, respectively. For KT40 and KLT40, a 4×4×4 Monkhorst-Pack k-point grid was used and for KLT80a, etc., a $2\times 2\times 2$ grid (Results for KLT80a are negligibly different with a $4\times 4\times 4$ Monkhorst-Pack grid).

This computational scheme was tested on pure KT with 5 atoms per cell. The self-consistent lattice constant $a = 3.96$ Å (Fig. 2) agrees with previous LDA and GGA computations[29]. The calculated lattice constant is smaller than the experimental value $a = 3.983$Å [28],

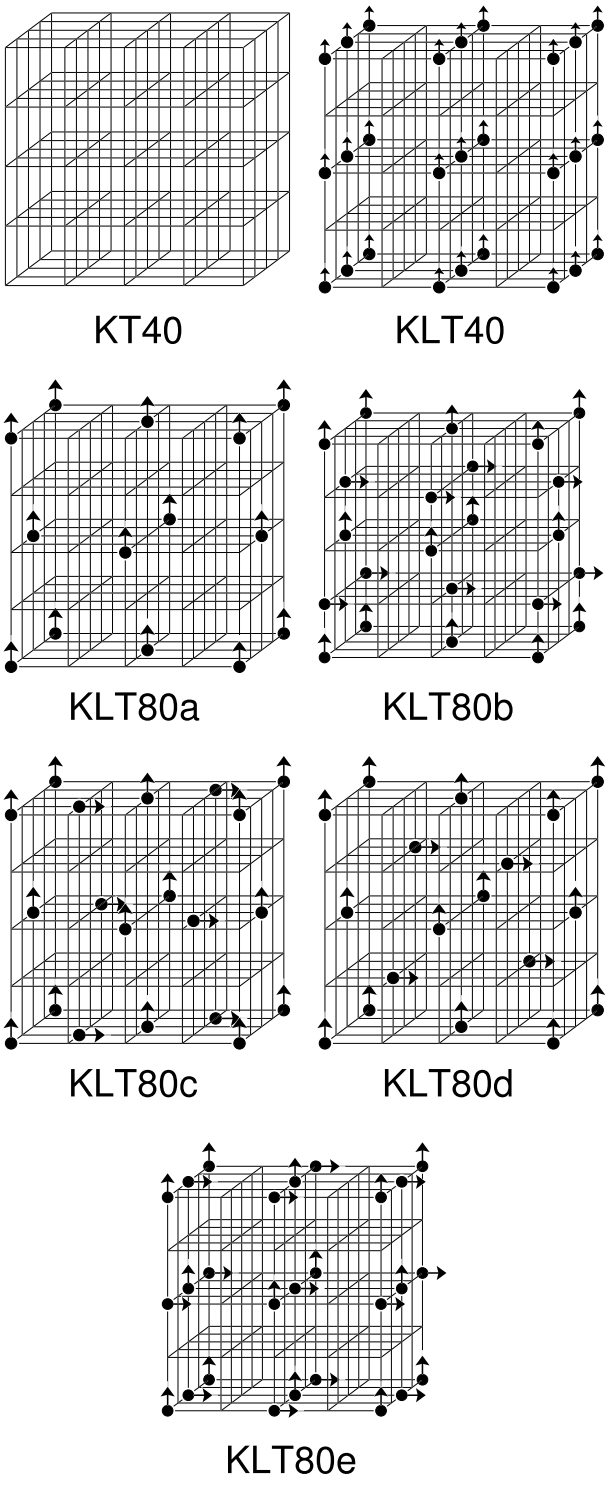

FIG. 1: KLT configurations on a 320-atom supercell. The grid connects perovskite A-sites. Empty sites represent K; black circles represent Li. When there is one Li per primitive cell, it is arbitrarily displaced in the $\hat{z}$ direction; when there are two Li per primitive cell, one is displaced in the $\hat{z}$ direction and the other in the $\hat{x}$ direction.

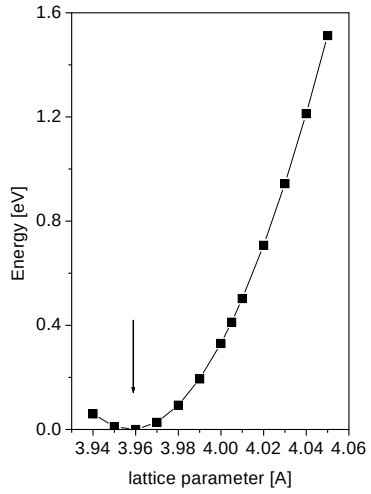

FIG. 2: Total energy as a function of lattice parameter in KLT40, cubic symmetry constraint.

which is a general feature of the LDA[29].

III. RESULTS

A Reference Structures

To study Li off-centering, one needs a reference structure in which Li occupies an ideal centrosymmetric A-site. This reference structure, $KLT40_{Ref}$, is obtained by placing all ions of KLT40 on ideal perovskite positions and optimizing lattice parameters and internal coordinates (except Li), subject to a cubic symmetry constraint. The resulting cell has $a = 2 \times 3.956$ Å. Crystallographic data for $KLT40_{Ref}$, are tabulated in Table I. Because Li is smaller than K, there is a volume contraction around Li-ions such that: nn Ta ions displace by 0.010 Å toward Li, and nn O ions displace by 0.024 Å, also towards Li.

TABLE I: Calculated structure for KLT40 with Li occupying ideal A-site positions, and the structure relaxed, subject to a cubic symmetry constraint. Space group $Pm\overline{3}m$; $a = 2 \times 3.9559$ Å.

ion	Wyckoff position	x	y	z
K_1	1a	0.0000	0.0000	0.0000
K_2	3d	0.0000	0.0000	0.5000
K_3	3c	0.5000	0.5000	0.0000
Li	1b	0.5000	0.5000	0.5000
Ta	8g	0.2508	0.2508	0.2508
O_1	12i	0.2509	0.2509	0.0000
O_2	12j	0.2522	0.2522	0.5000

A series of $KLT40_{Ref}$ frozen phonon calculations, with each symmetry-independent ion displaced in turn, was used to compute force constants, construct the dynamical matrix, and compute zone-center normal mode frequencies and eigenvectors. Symmetry analysis of $KLT40_{Ref}$ zone-center phonons yields $3A_{1g} + 2A_{2g} + 3A_{2u} + 5E_g + 3E_u + 5F_{1g} + 14F_{1u} + 6F_{2g} + 7F_{2u}$. Normal mode frequencies are listed in Table II. One zone-center instability is found for KLT40, with symmetry F_{1u}. Thus, as expected, the high-symmetry reference structure is dynamically unstable. Table III, gives the F_{1u} instability eigenvector, which is dominated by a Li off-centering [00d] displacement.

TABLE II: Computed normal mode symmetries and frequencies (ν in cm^{-1}) for $KLT40_{Ref}$ (Table I). Also listed are relative amplitudes a_{rel} for each mode in the fully relaxed tetragonal KLT40 structure. F_{1u} frequencies are for transverse optical modes, except for the zero-frequency acoustic mode.

symm.	ν	a_{rel}	symm.	ν	a_{rel}	symm.	ν	a_{rel}
A_{1g}	211	0.0906	F_{1g}	70	0.0000	F_{2g}	63	0.0000
A_{1g}	418	0.0877	F_{1g}	205	0.0000	F_{2g}	178	0.0000
A_{1g}	445	0.0504	F_{1g}	338	0.0000	F_{2g}	262	0.0000
			F_{1g}	527	0.0000	F_{2g}	327	0.0000
A_{2g}	167	0.0000	F_{1g}	611	0.0000	F_{2g}	534	0.0000
A_{2g}	285	0.0000				F_{2g}	910	0.0000
			F_{1u}	172 i	2.9599			
A_{2u}	58	0.0000	F_{1u}	0	0.0000	F_{2u}	129	0.0000
A_{2u}	507	0.0000	F_{1u}	120	0.3047	F_{2u}	159	0.0000
A_{2u}	945	0.0000	F_{1u}	164	0.0596	F_{2u}	178	0.0000
			F_{1u}	177	0.0080	F_{2u}	243	0.0000
E_g	125	0.6230	F_{1u}	187	0.2049	F_{2u}	256	0.0000
E_g	213	0.1954	F_{1u}	200	0.0082	F_{2u}	331	0.0000
E_g	279	0.2125	F_{1u}	205	0.2038	F_{2u}	349	0.0000
E_g	422	0.1413	F_{1u}	244	0.0961			
E_g	448	0.1241	F_{1u}	336	0.0901			
			F_{1u}	364	0.0041			
E_u	69	0.0000	F_{1u}	432	0.0373			
E_u	495	0.0000	F_{1u}	555	0.0378			
E_u	577	0.0000	F_{1u}	862	0.0075			

For comparison, the force constants of a 40-atom cell of pure $KTaO_3$ (KT40) were calculated at the same lattice parameter. The TO normal mode results are listed in Table IV. The force constants for KT40 and $KLT40_{Ref}$ are nearly identical. The only interatomic force constants that change by more than 0.41 eV/Å^2 are those involving the 12 O-ions that are nn of Li. For example, the radial interionic force constant between an A-ion and a nn-O changes sign from -0.21 eV/Å^2 in KT to $+0.74$ eV/Å^2 in $KLT40_{Ref}$ when K is replaced by Li. A positive sign for this term in $KLT40_{Ref}$ implies that Li-motion in opposition to its nn O-ions is energetically favorable. Thus, the single lattice instability in $KLT40_{Ref}$ is dominated by Li-motion (85% of the dynamical matrix eigenvector) opposite its nn O (12% of the dynamical matrix eigenvector). Because $KLT40_{Ref}$ and KT40 have such

TABLE III: Dynamical matrix eigenvector for the z-polarized 172 i cm^{-1} mode. Ionic labels correspond to those in table I.

ion	x	y	z	e_x	e_y	e_z
K_1	0.0000	0.0000	0.0000	0.0000	0.0000	0.0206
K_2	0.0000	0.0000	5.0000	0.0000	0.0000	-0.0374
K_2	0.5000	0.0000	0.0000	0.0000	0.0000	0.0036
K_3	0.5000	0.5000	0.0000	0.0000	0.0000	0.0507
K_3	0.0000	0.5000	0.5000	0.0000	0.0000	-0.0350
Li	0.5000	0.5000	0.5000	0.0000	0.0000	0.9252
Ta	0.2508	0.2508	0.2508	0.0300	0.0300	0.0252
O_1	0.2509	0.2509	0.0000	0.0000	0.0000	-0.0509
O_1	0.0000	0.2509	0.2509	-0.0187	0.0000	-0.0301
O_2	0.2522	0.2522	0.5000	0.0000	0.0000	-0.0242
O_2	0.5000	0.2522	0.2522	0.0000	-0.0649	-0.0875

similar force constant matrices, their normal mode spectra are very similar. Note that each TO mode in KT40 has a corresponding TO mode of very similar frequency in KLT40$_{\rm Ref}$.[30]

TABLE IV: Computed TO normal mode frequencies (ν in cm^{-1}) and dynamical matrix eigenvectors for $KTaO_3$ at $a = 3.956$ Å.

ν	u_K	u_{Ta}	$u_{O\parallel}$	$u_{O\perp}$
115	–0.2989	0.5419	–0.3937	–0.4807
205	0.8745	-0.1737	–0.2401	–0.2715
555	0.0012	0.0341	–0.8531	0.3682

B Fully Relaxed Structures

Full ionic relaxation in KLT40 indicates that (consistent with previous unrelaxed computations[20,21]) maximum energy reduction occurs when Li-ions are displaced to [00d] (Fig. 3). The calculated equilibrium Li-displacement (d) is d=1.009 Å (Table V), whereas fits to experimental data yield d=1.26 Å [2]. For comparison, the curves obtained when all ions, except for Li are fixed, are also shown in Fig. 3. Clearly, the depth of the well and the magnitude of Li-displacement are sensitive to relaxations of the surrounding ions.

The largest sympathetic distortion associated with Li-displacements involve the six nn O-ions (see Table V and Fig. 4), which are displaced towards Li by 0.109 Å. This large displacement is similar to what occurs in $LiNbO_3$ and $LiTaO_3$[31]. It is also consistent with the results of diffuse scattering studies of KLT[32] which indicate strongly correlated planar atomic displacements.

The results listed in Table V indicate that Ta-ions are generally displaced in the same direction as Li, while O-ions shift in the opposite direction. This is consistent with the view that Li-displacement leads to freezing of a soft-mode polarization fluctuation that has a large correlation radius.

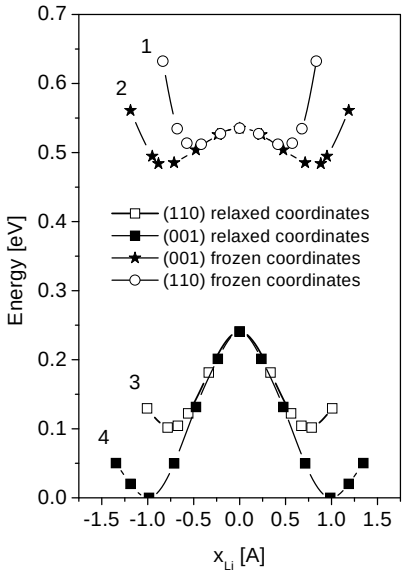

FIG. 3: Energy as a function of Li-displacement from an ideal A-site position in KLT40: Li displaced along 001 (1) and 110 (2), with all other ions frozen in their KLT40$_{\rm Ref}$ positions; Li displaced along 001 (3) and 110 (4), followed by full relaxations of all other ions.

A breakdown of the displacement pattern into normal mode coordinates for KLT40$_{\rm Ref}$ is shown in Table II. Anharmonic coupling leads to some contributions from higher frequency modes, but otherwise, the displacement pattern is dominated by the eigenvector of the lattice in-

TABLE V: Computed fully relaxed structure of KLT40. Space group P4mm; $a = 2 \times 3.9565$ Å; $c = 2 \times 3.9638$ Å; $c/a \approx 1.002$. Deviations are relative to positions in KLT40$_{\rm Ref}$. The origin is chosen so that both structures have the same center of mass.

ion	Wyckoff pos.	x	y	z	δx, Å	δy, Å	δz, Å
K_1	1a	0.0000	0.0000	0.0014	0.000	0.000	0.011
K_2	2c	0.5000	0.0000	0.9996	0.000	0.000	-0.003
K_3	2c	0.5000	0.0000	0.4963	0.000	0.000	-0.029
K_4	1a	0.0000	0.0000	0.4952	0.000	0.000	-0.038
K_5	1b	0.5000	0.5000	0.0074	0.000	0.000	0.058
Li	1b	0.5000	0.5000	0.6273	0.000	0.000	1.009
Ta_1	4d	0.2513	0.2513	0.2526	0.004	0.004	0.015
Ta_2	4d	0.2494	0.2494	0.7499	-0.011	-0.011	0.005
O_1	4d	0.2515	0.2515	0.9935	0.005	0.005	-0.051
O_2	4d	0.2474	0.2474	0.4957	-0.038	-0.038	-0.034
O_3	4e	0.0000	0.2500	0.2436	0.000	-0.007	-0.058
O_4	4e	0.0000	0.2533	0.7457	0.000	0.019	-0.027
O_5	4f	0.5000	0.2482	0.2442	0.000	-0.031	-0.063
O_6	4f	0.5000	0.2589	0.7379	0.000	0.053	-0.079

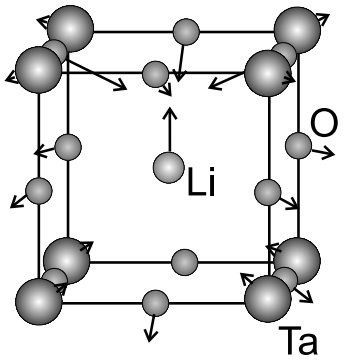

FIG. 4: Structural distortions around Li in KLT40.

stability. Vibrational frequencies for fully relaxed KLT40 were also calculated, and symmetry analysis of the fully relaxed tetragonal structure indicates that the phonon spectrum is 22 $A_1 + 8A_2 + 14B_1 + 12B_2 + 32E$. Modes belonging to irreducible representations A_1 and E are infrared active (except for the $A_1 + E$ acoustic set). The frequencies of infrared active modes are listed in Tables VI. Each column represents the (summed) projection (in percent) of the dynamical matrix eigenvector of relaxed KLT40 onto one (or more) eigenvectors of $KLT40_{Ref}$. If two eigenvectors were identical, the entry would be 100.

The KT soft-mode frequency, 120 cm^{-1}, splits into two modes in fully relaxed KLT40: E (123 cm^{-1}); A (161 cm^{-1}). Hence, the center of gravity for these modes is increased by Li-displacement as indicated by experimental data for hardening of the soft-mode in KLT[33]. However, only the component of the KT soft-mode triplet with polarization in the Li-displacement direction is significantly hardened. The Li-dominated instability of $KLT40_{Ref}$ undergoes mixing with several other modes of $KLT40_{Ref}$; its weighted average frequency is about 290 cm^{-1} in the polar direction and 330 cm^{-1} in the transverse directions.

A Computed averaged reflectivity spectrum for KLT40 is compared with one for KT in Fig. 5. The general structures of the two spectra are the same but in KLT40, KT-bands are split by symmetry-breaking Li-displacements.

C Isolated Li-Ions

Li-ions can jump between neighboring [0,0,d] wells via [110] saddle points. Figure 6 shows the computed Li potential between neighboring Li-wells; e.g. [0,0,d] and [0,d,0] via a minimum energy [011] saddle. The energetics for Li motion, with all ions except Li frozen, are constrasted with the energetics for Li motion with correlated relaxations of the other ions. Clearly, ionic relaxation promotes Li-hopping by reducing potential barriers. Fully relaxed calculations yield reasonable agreement with results obtained from Arrhenius fits to NMR data[2]. The fixed-ion potential barrier is ∼103 meV (1190

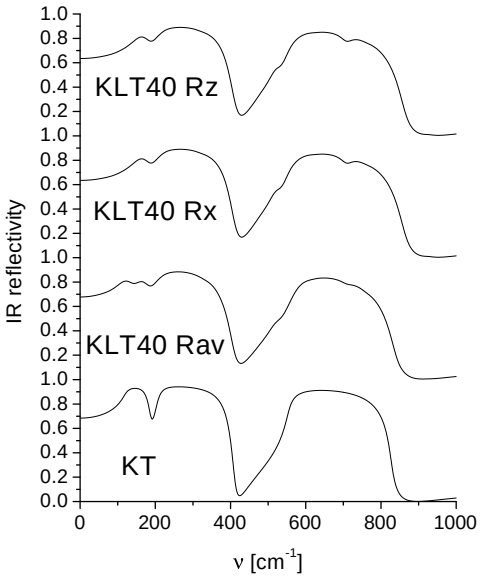

FIG. 5: Comparison of the reflectivity spectra computed for KT and KLT40 (the component along the polar axis (R_z), perpendicular to it (R_x), and averaged spectrum (R_{av})) at identical lattice parameters $a_0 = 3.956\mathring{A}$. The electronic permittivity ε_∞ was set to 5.15 in each case, the experimental value for KT.[34] The damping constant was set to 20 cm^{-1} for all modes in KT and 40 cm^{-1} for KLT40.

K). The experimental value, 86 meV (1000 K) [3] is lower but the value 103 meV (1200 K) is close. A similar potential barrier value was also obtained in the KLT80a computation. Note that computed barrier heights will be systematically larger than values obtained by experiment if the latter are reduced by Li-tunneling over excited states.

D Li-Li Pairs

The energetics of Li-Li nn pair displacement configurations were studied with 80 atom supercell calculations (Fig. 7)) for all nn-pair configurations listed in Table VII. Fully relaxed total energy calculations indicate that the lowest energy path for converting the minimum energy $z - z$ configuration into the $\overline{z} - \overline{z}$ configuration is via intermediate microstates: e.g. the energy for $z - z \rightarrow x - y$ is 2627 K (Table VIII) in qualitative agreement with the barrier height, 2100-2800 K,[11–13] attributed to the rearrangement of Li-Li nn-pairs.[10] Barrier height computations for two selected low-energy paths (see Fig. 8) were performed by converting the $z-z$ configuration into $\overline{z} - \overline{z}$ via intermediate states (Fig. 7). Note that the metastable states are separated by high

TABLE VI: Computed TO normal mode frequencies (ν in cm^{-1}) for modes of symmetry E (left) and A_1 (right) in fully relaxed KLT40. Also shown is the squared projection (in percent) of the eigenvector of each mode onto an eigenvector, or set of eigenvectors, of the dynamical matrix for $KLT40_{Ref}$. (1) The $127i$ cm^{-1} instability, (2) the 120 cm^{-1} mode similar to the KT40 soft-mode. (3) All other polar eigenvectors and (4) All nonpolar eigenvectors.

ν	(1)	(2)	(3)	(4)	ν	(1)	(2)	(3)	(4)
65	0.2	0.5	0.1	99.2	148	0.5	4.8	15.2	79.5
77	0.1	0.3	0.1	99.5	161	0.9	84.3	8.7	6.0
123	7.0	89.2	1.1	2.7	168	0.1	0.4	88.9	10.5
145	0.0	0.8	0.7	98.5	177	6.4	1.0	87.5	5.1
160	0.0	0.0	1.1	98.8	183	0.3	0.2	94.3	5.2
161	0.3	0.8	98.3	0.6	199	2.1	0.5	96.9	0.5
176	0.0	0.3	24.8	74.8	207	5.1	2.8	66.3	25.8
178	0.0	0.1	78.7	21.2	212	1.2	0.9	7.1	90.8
188	0.9	0.8	92.5	5.8	215	0.6	2.6	25.4	71.3
199	0.3	0.3	94.6	4.8	242	7.2	0.0	88.5	4.3
200	0.4	0.4	48.3	50.9	282	16.2	0.5	11.7	71.5
206	2.5	1.1	47.2	49.3	300	47.0	1.5	16.0	35.5
224	0.1	0.1	10.0	89.9	336	2.3	0.1	96.4	1.2
240	3.3	0.4	79.8	16.5	366	1.6	0.1	93.4	5.0
248	0.4	0.0	1.5	98.1	418	0.1	0.0	23.9	76.0
254	4.3	0.2	16.0	79.5	430	4.8	0.0	1.4	93.8
262	0.0	0.0	0.8	99.2	444	0.3	0.0	64.6	35.1
321	40.9	2.7	32.7	23.7	451	3.2	0.1	0.8	95.9
333	2.7	0.2	3.9	93.2	459	0.0	0.0	13.7	86.2
334	1.0	0.1	11.2	87.8	570	0.1	0.3	99.5	0.2
336	1.2	0.1	68.4	30.3	872	0.0	0.0	99.6	0.4
342	0.0	0.0	25.1	74.9					
351	0.4	0.0	4.9	94.6					
399	32.2	1.7	59.2	6.9					
434	1.1	0.1	98.2	0.6					
529	0.1	0.0	15.3	84.6					
547	0.0	0.0	5.4	94.6					
563	0.2	0.0	79.5	20.3					
625	0.0	0.0	0.6	99.4					
859	0.0	0.0	99.6	0.3					
914	0.1	0.0	0.3	99.6					

TABLE VII: Fully relaxed Li-Li nn-pair configurations in KLT80b ($a = 4$ Å)

notation	x_1	y_1	z_1	x_2	y_2	$z_2 - a$	$E[eV]$
$z-z$	0.00	0.00	1.43	0.00	0.00	1.19	0.000
$x-\overline{x}$	1.10	0.00	–0.01	–1.10	0.00	0.01	0.279
$x-\overline{z}$	1.11	0.00	–0.02	0.00	0.00	−1.12	0.221
$x-x$	1.07	0.00	0.00	1.07	0.00	0.00	0.257
$x-z$	1.18	0.00	0.06	–0.01	0.00	1.31	0.124
$z-\overline{z}$	0.00	0.00	0.76	0.00	0.00	−0.76	0.550
$y-x$	0.00	1.12	–0.01	1.12	0.00	0.01	0.227
$\overline{z}-z$	0.00	0.00	–1.09	0.00	0.00	1.09	0.335

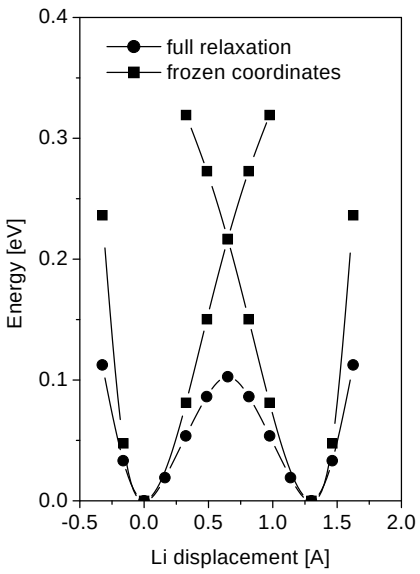

FIG. 6: Li potentials obtained with full relaxation of non-Li ions, and with fixed coordinates for non-Li ions in KLT40. The path between neighboring [00d]-type Li-wells is via a [110]-type saddle point.

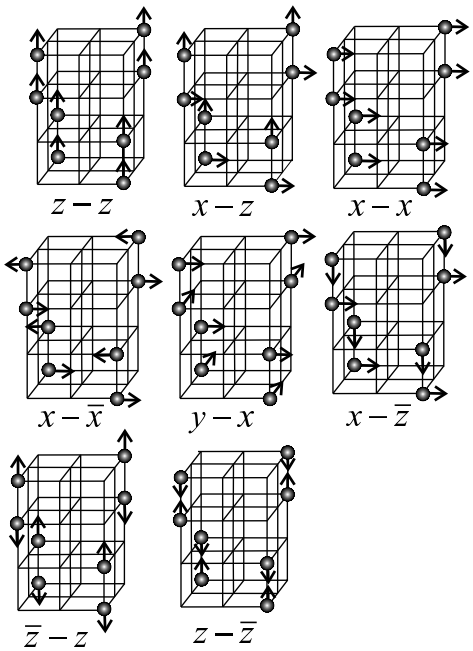

FIG. 7: A-site configurations in KLT80b. Undecorated sites are occupied by K. See Table VII for explanations of notation.

TABLE VIII: Excitation energies for Li-Li nn-pairs (K).

notation	$z-z$	$x-z$	$x-\overline{z}$	$y-x$	$x-x$	$\overline{z}-z$	$x-\overline{x}$	$z-\overline{z}$
$z-z$	0							
$x-z$	1432	0						
$x-\overline{z}$	2570	1138	0					
$y-x$	2627	1195	57	0				
$x-x$	2990	1558	420	363	0			
$x-\overline{x}$	3170	1738	600	543	180	0		
$\overline{z}-z$	3883	2451	1313	1253	893	713	0	
$z-\overline{z}$	6379	4947	3809	3752	3389	3209	2496	0

TABLE IX: Fully relaxed Li-Li second nearest neighbor pair configurations (KLT80c) ($a = 4$ Å).

notation	x_1	y_1	z_1	x_2-a	y_2-a	z_2	$E[eV]$
$x-x_2$	1.14	0.01	–0.01	1.13	0.01	–0.01	0.141
$z-z_2$	0.00	–0.03	1.09	0.00	-0.00	1.09	0.275
$z-\overline{z}_2$	0.00	0.00	1.14	0.00	-0.00	–1.16	0.235
$x-z_2$	1.11	0.00	–0.02	0.03	0.00	1.13	0.213
$\overline{x}-z_2$	–1.13	0.00	–0.01	–0.01	0.02	1.14	0.211
$x-\overline{x}_2$	1.10	-0.02	-0.00	-1.18	-0.05	0.01	0.383
$\overline{x}-y_2$	–1.11	0.03	-0.01	–0.02	1.11	–0.01	0.216
$x-\overline{y}_2$	1.11	–0.02	0.01	0.02	–1.11	0.01	0.216
$x-y_2$	1.14	0.03	–0.01	0.04	1.14	–0.02	0.258

TABLE X: Fully relaxed Li-Li third nearest neighbor pair configurations (KLT80d) ($a = 4$ Å)

notation	x_1	y_1	z_1	x_2-a	y_2-a	z_2-a	$E[eV]$
$z-z_3$	–0.01	0.00	1.14	-0.01	0.00	1.14	0.138
$z-x_3$	0.03	0.01	1.12	1.12	–0.02	0.03	0.229
$z-\overline{z}_3$	0.01	–0.01	1.09	0.02	–0.02	–1.19	0.387
$\overline{z}-z_3$	0.01	–0.01	–1.09	0.00	0.00	1.09	0.385

TABLE XI: Fully relaxed Li-Li fourth nearest neighbor pair configurations (KLT80e) ($a = 4$ Å).

notation	x_1	y_1	z_1	x_2	y_2	z_2-2a	$E[eV]$
$z-z_4$	0.00	0.00	1.09	0.00	0.00	1.08	0.248
$z-\overline{z}_4$	0.00	0.00	1.10	0.00	0.00	–1.10	0.257
$z-x_4$	–0.02	0.00	1.14	1.11	0.00	–0.01	0.213

barriers the lowest of which, 356 meV (4130 K), is significantly larger than the value 2100-2800K[11–13] obtained by fitting an Arrhenius expression to experimental data; this discrepancy may be explained by Li-tunneling between metastable states.

Significantly, the excitation energy for $z-z \rightarrow x-x$ Li-Li nn-pair flipping is close to the energy for $z-z \rightarrow x-\overline{x}$ and $\overline{z}-\overline{z} \rightarrow x-y$ flipping. These results contradict both the classic dipole-dipole interaction expression, and the modified expression derived by Vugmeister and Glinchuk[4] (see also Refs. [35,36]), which includes spherically symmetric soft-mode dispersion. There is a strong angular dependence of the soft-mode frequency[37], so the assumption of spherical symmetry is not justified, and local anisotropy of the lattice dynamics, caused by Li-displacements, should be taken into account.

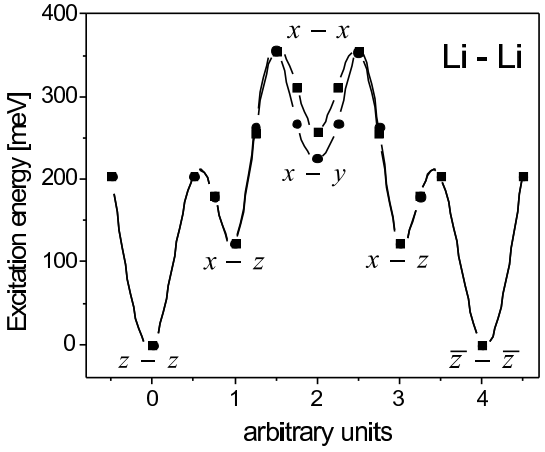

FIG. 8: The energetics of Li-Li nearest neighbor pair reorientation, $z-z \rightarrow \overline{z}-\overline{z}$, including the intermidiate states depicted in Fig. 7.

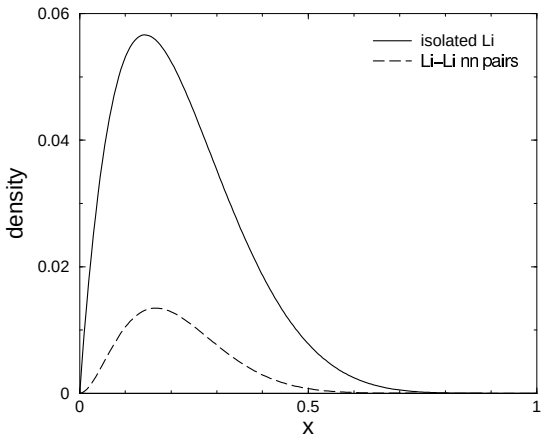

FIG. 9: Densities per A-site of isolated Li-ions and Li-Li nearest-neighbor pairs in $K_{1-x}Li_xTaO_3$, as fuctions of x .

If the experimental observation of two relaxation processes[11,12] corresponds to flipping of isolated Li-ions and Li-Li nn-pairs, respectively, then significant concentrations of both must be present. Assuming a random distribution of Li-ions in KLT, one can calculate the densities of isolated Li-ions and Li-Li nn pairs as functions of x. The results are shown in Figure 9. Note (1) significant concentrations of both isolated Li and Li-Li nn pairs are present at values of x where two relaxation processes are observed; (2) the relative concentrations of Li-Li nn pairs is low for $0 < x < 0.02$ where only one relaxation process is observed.

Results for supercells with two Li-ions separated by distances greater than a_0 are given in Tables IX-XI. For instance, KLT80e has three symmetry-independent con-

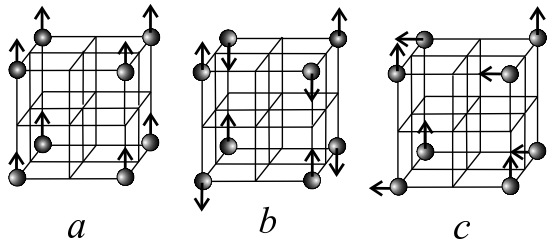

FIG. 10: Fourth nearest neighbor Li-Li configurations: a) $(z - z_4)$; b) $(z - \overline{z}_4)$, and c) $(z - x_4)$.

figurations (Fig. 10): (1) both Li-ions are displaced in the same direction, $z - z_4$; (2) they are displaced in opposite directions; $z - \overline{z}_4$; (3) they are displaced in perpendicular directions, $z - x_4$. The $z - x_4$ configuration has lowest energy; $z - z_4$ is 34 meV higher, and $z - z_4$ is 9 meV higher than $z - z_4$. These results are in qualitative agreement with shell model computations[38] that indicate a tendency for the formation of $z....x$ configurations, but at greater Li-Li separations than 4'th nn. Note, however, that this result only holds for cubic supercells, as shown below, tetragonal distortion of the structure stabilizes the $z - z_4$ configuration.

E Dynamical Charges and Polarization

TABLE XII: Dynamical charges Z^*_{zz} in the KLT40 supercell.

Ions	x	y	z	Z^*_{zz}	Z^*_{xx}	Z^*_{yy}	
K_1	1a	0.0000	0.0000	0.0014	1.117	1.143	1.143
K_2	2c	0.5000	0.0000	0.9996	0.671	1.181	1.133
K_3	2c	0.5000	0.0000	0.4963	0.660	1.169	1.123
K_4	1a	0.0000	0.0000	0.4952	0.644	1.147	1.147
K_5	1b	0.5000	0.5000	0.0074	1.071	1.178	1.178
Li	1b	0.5000	0.5000	0.6273	0.549	1.106	1.106
Ta_1	4d	0.2513	0.2513	0.2526	7.976	8.746	8.746
Ta_2	4d	0.2494	0.2494	0.7499	8.478	8.480	8.480
O_1	4d	0.2515	0.2515	0.9935	–6.712	–1.683	–1.683
O_2	4d	0.2474	0.2474	0.4957	–6.955	–1.637	–1.637
O_3	4e	0.0000	0.2500	0.2436	–2.180	–6.379	–1.736
O_4	4e	0.0000	0.2533	0.7457	–2.114	–6.355	–1.617
O_5	4f	0.5000	0.2482	0.2442	–2.103	–6.659	–1.642
O_6	4f	0.5000	0.2589	0.7379	–2.067	–6.194	–1.788

The polarization induced by Li off-centering was studied by Berry's phase analyses, and dynamical charges $Z^*_{\alpha\alpha}$ were determined for all ions in $KLT40_{\rm Ref}$, fully relaxed KLT40 (Table XII), and KLT40 with ions in ideal perovskite positions (Table XIII). Compare these charges with Z_{zz} in KT with the same lattice parameter: K. 1.151; Ta. 8.680; Ox. -1.690; Oy. -1.690; Oz. -6.452.

The dynamical charge is a symmetric function of displacements (u) from ideal perovskite positions, so to a first approximation, it is quadratic in u:

$$Z^*_{zz}(u) = Z^*_{zz}(0) - \zeta u^2 \tag{1}$$

The average dynamical charge, which is required for calculating the polarization, is

$$\langle Z^*_{zz}\rangle = \frac{1}{u_1 - u_0}\int_{u_0}^{u_1} Z^*_{zz}(u)du = $$

$$= Z^*_{zz}(0) + \frac{1}{3}\zeta\left(u_1^2 + u_0^2 + u_1u_0\right) \tag{2}$$

In particular, if $u_0 = 0$ then

$$\langle Z^*_{zz}\rangle = \frac{1}{3}\left(Z^*_{zz}(u) + 2Z^*_{zz}(0)\right) \tag{3}$$

Average values of the dynamical charges, and individual ion contributions to the total KLT40 supercell dipole moment are listed in Table XIII. For comparison, the explicit value of the total dipole moment, obtained by Berry phase analysis, is also shown.

The largest contribution to the total dipole moment is from O ions. The Li-displacement contribution is approximately equal to that of Ta. The total dipole moment is ∼5 times larger than the Li-dipole moment, which indicates that the Li-dipole moment is strongly *enhanced* by structural relaxation.

TABLE XIII: Dynamical charges Z^*_{zz}, ionic displacements (in Å) and total dipole moment (in eÅ) in the KLT40 supercell. Only symmetrically distinct ions are listed: for ionic coordinates see Table V.

Ions	Refer. struct.	Ideal perov. struct	Average dyn.ch.	Displ. [Å]	Tot.dip. [eÅ]
K_1	1.154	1.151	1.140	0.021	0.024
K_2	1.154	1.150	0.990	0.007	0.014
K_3	1.154	1.152	0.988	-0.019	-0.038
K_4	1.154	1.152	0.983	-0.028	-0.028
K_5	1.154	1.123	1.106	0.069	0.076
all K			1.026	0.005	0.048
Li	1.251	1.251	1.017	1.017	1.034
Ta_1	8.713	8.710	8.465	0.029	0.982
Ta_2	8.714	8.712	8.634	0.008	0.276
all Ta			8.550	0.019	1.258
O_1	-6.448	-6.474	-6.553	-0.037	0.970
O_2	-6.527	-6.506	-6.656	-0.020	0.532
			-6.605	-0.029	1.502
O_3	-1.702	-1.702	-1.861	-0.038	0.283
O_4	-1.699	-1.702	-1.839	-0.020	0.147
O_5	-1.686	-1.686	-1.825	-0.031	0.226
O_6	-1.686	-1.686	-1.813	-0.083	0.602
			-1.835	-0.043	1.258
all O					2.760
Total					5.100
Exact	value				5.153

A similar enhancement was also obtained in a shell model calculation,[39] but in that study the main cause of enhancement was a large Ta-displacement. Here, enhancement of the Li-dipole moment is primarily caused by coupling between Li- and O-displacements.

TABLE XIV: The KLT80b supercell dipole moment for different Li-Li nn-pair configurations

notation	direction	K	Li	Ta	$O_\perp$	$O_\parallel$	Total
$z-z$	z	0.124	2.667	4.608	2.416	3.994	13.809
$x-\overline{z}$	z	-0.153	-1.159	-3.680	-1.562	-2.618	-9.172
	x	0.301	1.129	4.886	1.183	1.958	9.457
$x-x$	x	0.353	2.167	5.647	2.267	3.545	13.979
$x-z$	z	0.137	1.397	3.807	1.294	2.284	8.919
	x	0.460	1.184	6.227	0.632	1.046	9.549
$y-x$	y	0.353	1.138	5.418	0.945	1.535	9.387
	x	0.353	1.138	5.418	0.945	1.535	9.387

Total dipole moments for a KLT80b supercell with different Li-Li nn-pair configurations are listed in Table XIV. They were calculated with the average dynamical charges listed in Table XIII and ionic displacements relative to ideal perovskite. Individual ionic contributions are also shown. Oxygen ion contributions are separated into $O_\parallel$ and $O_\perp$, with the polarization direction parallel and perpendicular to the Ta-O-Ta bond, respectively. These results indicate that the total dipole moment induced by Li-Li pairs is much larger than that from two isolated Li-ions.

F Coupling Between Strain and Polarization

The influence of applied stress on dipole moment was studied by applying various tetragonal distortions to the KLT40 supercell with $a = 3.95594$ Å, and $0.98a < c < 1.02a$. Total energy calculations show that, for $c > a$, configurations with [001]-displaced Li-ions are lower in energy than those with [100]-displaced Li:

$$-\delta E_{zz}[meV] = 1.649s + 105.7s^2 + 3430s^3 \qquad (4)$$

where $s = (c/a - 1)$. The occupation probability for Li-displacements in the c-direction can be estimated as

$$w_{-z-z} = w_{zz} = \frac{e^{-\delta E_{zz}/k_BT}}{4 + 2e^{-\delta E_{zz}/k_BT}} \approx 1/6 - \delta E_{zz}/24k_BT \qquad (5)$$

Hence, tetragonal strain increases the population of Li-displacements parallel to the c-axis. The energy decrease connected with redirected Li-ions is,

$$< \delta E_{Lizzzz} >= n_{Li}\delta E_{zz}(w_{-z-z} + w_{zz} - 1/3) \approx -n_{Li}\delta E_{zz}\delta E_{zz}/12k_BT \qquad (6)$$

which at small s, is proportional to s^2; n_{Li} is the concentration of Li per primative unit cell. Thus, the structure is softened by local Li-redirections.

Li-redirection also increases the square of local polarization along the c-axis

$$\delta q_{zzzz} = p_{Liz}p_{Liz}(w_{zz} + w_{-z-z} - 1/3) \approx p_{Liz}p_{Liz}\delta E_{zz}/12k_BT \qquad (7)$$

where p_{Liz} is the z-component of Li-related local polarization. From comparison with (4) one sees that δq_{zzzz} is proportional to strain at small s. This is consistent with large electrostriction constants that are observed in paraelectric KLT at $50 < T < 100$ K [11]. Because Li-redirection is connected with hopping dynamics, one expects a relaxation contribution to the acoustic response, as observed by Pattnaik and Toulouse [40].

Using the average dynamical charges and computed ionic displacements, one can calculate supercell dipole moments, d_z and d_x, which correspond to Li-ions displaced in the [001] and [100] directions respectively, for $a < c < 1.2a$:

$$d_z[e\mathring{A}] = 5.15 + 167.s + 2987.s^2$$
$$d_x = 5.15 - 40.s + 585.s^2 \qquad (8)$$

These results show that the supercell dipole moment is greatly enhanced by an increase in the c-axis. Partial contributions to the dipole moment that are associated with Ta- and O-displacements are most sensitive to changes in c; which is consistent with an electrostriction induced reduction in the soft-mode frequency.

G Toward an Effective Hamiltonian

The picture of KLT in which Li-dopoles, a soft-mode, and PNC all interact, lends itself to a first-principles based effective Hamiltonian (H_{eff}) treatment. Full formulation of H_{eff} is beyond the scope of this work, but some essential intermediate results have been derived. For simplicity, consider KLT40, with the same ionic displacements in each unit cell.

To derive H_{eff} for a FE, one selects a local basis for the instabilities that cause the FE transition, and includes interactions between sites, between local distortion and strain, etc.[41]. In KLT, it is clear that instabilities centered on Li are responsible for the phase transition, and that Li-centered distortion variables must be included in H_{eff}. However, the coupling of Li-dipole moments to the KT soft-mode is sufficiently important that one must also include a local variable for the KT soft-mode. By analogy with H_{eff} for $KNbO_3$[42], this local variable is centered on the Ta sites.

Several eigenvectors are relevant:

- $v_{1,\alpha}$: the dynamical matrix eigenvector for the KT soft-mode, polarized along $\hat{\alpha}$.
- $v_{2,\alpha}$: the dynamical matrix eigenvector for the Li-instability of KLT40, polarized along $\hat{\alpha}$. (Dynamical matrix eigenvectors are normalized for 40-atom cells).
- $v_{Ta,\alpha} = v_{1,\alpha}$ and $v_{Li,\alpha} = v_{2,\alpha}$, orthogonalized to $v_{1,\alpha}$.
- $d_{Li,\alpha}$ and $v_{Ta,\alpha}$, the dimensionless displacement eigenvectors obtained by dividing the elements of $v_{Ta,\alpha}$ and $v_{Li,\alpha}$, respectively, by $\sqrt{(m/m_0)}$, where (arbitrarily) mass $m_0 = 1$ amu.

Consider displacement patterns in KLT40 in which the displacement amplitudes correspond to $v_{Ta,\alpha}$ and $v_{Li,\alpha}$ are τ_α and λ_α, respectively. The energy is minimized with respect to all other modes. The strain tensor is given by $\{e_i\}, i = 1,6$, in Voigt notation. Calculated results closely fit the expansion:

$$
\begin{aligned}
U = U_o \\
&- 0.055566|\lambda|^2 + 0.004160|\lambda|^4 \\
&+ 0.016303(\lambda_x^2\lambda_y^2 + \lambda_x^2\lambda_z^2 + \lambda_y^2\lambda_z^2) \\
&- 0.000077|\lambda|^6 + 0.000001|\lambda|^8 \\
&+ 0.024760|\tau|^2 + 0.008677|\tau|^4 \\
&- 0.011288(\tau_x^2\tau_y^2 + \tau_x^2\tau_z^2 + \tau_y^2\tau_z^2) + 0.000684|\tau|^6 \\
&- 0.025236\vec{\lambda}\cdot\vec{\tau} + 0.001210(\lambda_x^3\tau_x + \lambda_y^3\tau_y + \lambda_z^3\tau_z) \\
&- 0.000370(\lambda_x\tau_x(\lambda_y^2 + \lambda_z^2) + \text{cyclic perm.}) \\
&+ 817.342(e_1^2 + e_2^2 + e_3^2) + 210.580(e_1e_2 + e_1e_3 + e_2e_3) \\
&+ 732.803(e_4^2 + e_5^2 + e_6^2) \\
&- 0.262724(e_1\lambda_x^2 + e_2\lambda_y^2 + e_3\lambda_z^2) \\
&- 0.209816(e_1(\lambda_y^2 + \lambda_z^2) + e_2(\lambda_x^2 + \lambda_z^2) + e_3(\lambda_x^2 + \lambda_y^2)) \\
&- 5.30307(e_4\lambda_y\lambda_z + e_5\lambda_x\lambda_z + e_6\lambda_x\lambda_y) \\
&- 3.24098(e_1\tau_x^2 + e_2\tau_y^2 + e_3\tau_z^2) \\
&+ 0.715628(e_1(\tau_y^2 + \tau_z^2) + e_2(\tau_x^2 + \tau_z^2) + e_3(\tau_x^2 + \tau_y^2)) \\
&+ 1.38297(e_4\tau_y\tau_z + e_5\tau_x\tau_z + e_6\tau_x\tau_y),
\end{aligned}
\tag{9}
$$

where U is in eV and $\vec{\lambda}$ and $\vec{\tau}$ in Å.

The potential for $\vec{\lambda}$ alone ($\sim$ Li off-centering) has 6 wells in [001]-type directions. The potential for $\vec{\tau}$ alone (KT soft-mode) has a small positive harmonic coefficient and is therefore highly polarizable. Negative bilinear coupling between $\vec{\lambda}$ and $\vec{\tau}$ indicates that the soft-mode enhances the total polarization from Li off-centering. Positive coefficients of $|\tau|^4$ and $|\tau|^6$ mean that the soft-mode frequency hardens as the structure is distorted. Higher-order coupling between $\vec{\lambda}$ and $\vec{\tau}$ is included, because it significantly improves the fit.

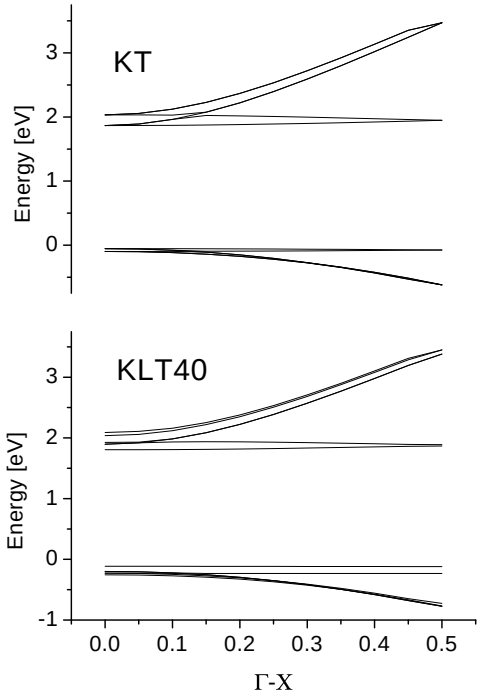

FIG. 11: Comparison of the electronic band structures in KT and KLT40

One can reduce the number of variables by excluding strain. This results in a decrease of the nonlinearity constant which multiplies the fourth power of polarization, and changes the sign of the angle dependent term for the soft-mode. Given only the soft-mode coordinate and the Li-displacements, one can find the soft-mode and Li-dipole contributions to the dielectric permittivity; Li-dipole contributions are mainly relaxational in nature (c.f. Sec IV).

To complete H_{eff} requires: (1) Formulating local representations of $\vec{\lambda}$ and $\vec{\tau}$ (*e.g.* lattice Wannier functions[43]); (2) Quantifying distance dependencies of the interactions[41,44].

H Band Structure Calculations

Strong n-type photocurrent is observed in KLT at $T \lesssim 80K$ [22], and it has been attributed to shallow hole states at the bottom of the valence band which are caused by large O_6-displacements. Holes are trapped by these levels which prevents recombination with electrons that were promoted to the conduction band by light absorption.

To study shallow forbidden gap states in KLT, band-structure calculations were performed for KLT40 and the corresponding ideal $KTaO_3$ supercell, in the $\Gamma - X$ di-

rection. Results for the valence and conduction bands are shown in Fig. 11. The top of the valence band, and the bottom of the conduction band, are split in KLT40 relative to KT.

Our results confirm large O_6-displacements[22], and demonstrate a large splitting at the top of the valence band, and at the bottom of the conduction band. This splitting occurs because Li off-centering breaks $Pm\overline{3}m$ symmetry creating symmetrically different O-ions with different self-consistent electrostatic potentials (c.f. Ref. [45]).

TABLE XV: Electrostatic potentials (in eV) on the ions of the KLT40 supercell. Only symmetrically distinct ions are listed (atomic positions are listed in Table V.

Ions	Equilibrium str.	Reference str.	ideal KT
K_1	10.151	10.177	10.331
K_2	10.133	10.145	10.331
K_3	10.176	10.226	10.331
K_4	10.154	10.145	10.331
K_5	10.136	10.226	10.331
Li	43.902	42.678	
Ta_1	-1.209	-1.219	-1.302
Ta_2	-1.290	-1.219	-1.302
O_1	-56.274	-56.260	-56.070
O_2	-56.295	-56.304	-56.070
O_3	-56.192	-56.260	-56.070
O_4	-56.457	-56.260	-56.070
O_5	-56.281	-56.306	-56.070
O_6	-56.430	-56.306	-56.070

Computing the electrostatic potentials on different ions in KLT40 (Table XV) reveals that the O_6 states are significantly deeper in fully relaxed KLT40 than in KT or in $KLT40_{Ref}$. The same result was obtained from projections of band states onto O_6 states. Without taking into account a polaronic contribution, O_6-states in KLT40 lie below the top of the valence band. Polaronic contributions to the energy should be studied separately.

Similar results are seen for Li-Li nn pairs (see Fig. 12), where the tetragonal distortion from Li-Li nn-pairs also causes valence and conduction band splitting but the $O-6$ related states again lie much lower than the top of the valence band. Thus, another mechanism might be responsible for the observed photocurrent. Our computations show that the band splitting is mainly caused by the electrostatic potential and this result is consistent with the model described in Ref. [45].

IV. PHENOMENOLOGY

Isolated Li-ion hopping in a cubic environment is associated with *two* relaxation processes, that have distinct relaxation times.[2] The first process has T_{1u} symmetry ($\tau^{-1} = 4k$ where k is the rate of successful hopping between adjacent sites), and couples with an electric field;

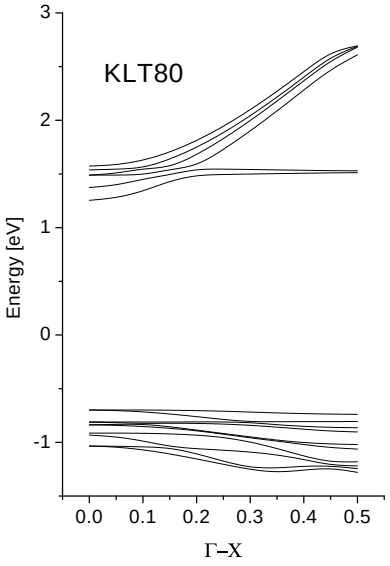

FIG. 12: Band structure of KLT80 with a $z-z$ Li nn-pair. The valence states are below zero energy.

so it can affect dielectric dispersion. The second process has e_g symmetry ($\tau^{-1} = 6k$), and couples with stress, but not with electric field.

If the crystal (or domain) is tetragonally distorted then there are four relaxation times: $\tau^{-1} = 4k_1;\ 4k_2;\ 6k_2;\ 2k_2 + 4k_1$ where k_1 and k_2 are the rates of successful hopping between adjacent sites (one, or neither of which, respectively, involves a hop parallel to the c-axis). The first two (A_1 and E symmetry) can couple to polarization, and the latter two can couple to stress, but not polarization. Applying a tensile tetragonal stress reduces the degeneracy of lowest energy Li off-center states from six ($\pm x,\ \pm y,\ \pm z$) to two z and $-z$ (the transversely oriented wells have higher energies as shown in Sec. III F). In principle, tetragonal distortion might explain experiments that indicate two relaxation processes: one relaxation process might be connected with tetragonally less distorted unit cells and the other with strongly distorted cells. The latter occurs at Li-Li nn-pairs where there are only two low lying states: zz; and $\overline{zz}$. Hence, a plausible explanation for two relaxation processes is that one is associated with reorientations of isolated Li-ions, and the other with Li-Li nn-pairs.

Consider the effect of Li-Li nn-pairs on the distribution of relaxation times. For simplicity, consider only the states in one of the paths that are shown in Figure 8. The corresponding kinetic equations are:

$$-\frac{dw_a}{dt} = k_{ab}w_a - k_{ba}w_b$$

$$-\frac{dw_b}{dt} = (k_{ba}+k_{bc})w_b - k_{ab}w_a - k_{cb}w_c$$
$$-\frac{dw_c}{dt} = 2k_{cb}w_c - k_{bc}w_b - k_{bc}w_d$$
$$-\frac{dw_d}{dt} = (k_{bc}+k_{ba})w_d - k_{cb}w_c - k_{ab}w_e$$
$$-\frac{dw_e}{dt} = k_{ab}w_e - k_{ba}w_d \quad (10)$$

where w_α is occupation probability for well α. Relaxation times can be obtained explicitly:

$$\tau_{1,2}^{-1} = a/2 \pm \sqrt{b^2 - k_{ba}(2k_{cb}-k_{ab})}$$
$$\tau_{3,4}^{-1} = (k_{ab}+k_{ba}+k_{bc})/2 \pm \sqrt{c^2 + k_{ab}k_{ba}} \quad (11)$$

Here $a = (k_{ab}+k_{ba}+k_{bc}+2k_{cb})/2$, $b = (k_{ba}+k_{bc}+2k_{cb}-k_{ab})/2$ and $c = (k_{ba}+k_{bc}-k_{ab})/2$.

The description is especially simple in the realistic limit $k_{ab} \sim k_{bc} \ll k_{cb} \sim k_{ba}$: $\tau^{-1} \simeq k_{ba}; 2k_{ba}; k_{ba}; k_{bc}k_{ab}/k_{ba}$. Only the last solution, which corresponds to overcoming the principle Li-Li nn-pair barrier ($z-z \to x-x$) in the $z-z \rightleftharpoons \overline{z}-\overline{z}$ process is essential for explaining the dielectric permittivity of the ground state. Assuming that the experimentally observed slow relaxation process (2100-2700 K[11,12]) derives from $z-z \rightleftharpoons \overline{z}-\overline{z}$, Li-Li nn-pair-flipping, only one relaxation time for each possible path is predicted, $k_{ba}/k_{ab}k_{bc}$. The other, much faster, rates correspond to processes of decaying excited metastable states (e.g. $x-x \to x-\overline{z}$ and $x-\overline{z} \to \overline{z}-\overline{z}$) that only occur if special initial conditions are satisfied; e.g. if metastable excited states are populated as a consequence of infrared, or acoustic, absorbtion. Excitation energies for all 36 Li-Li nn-pair transitions are listed in Table VIII.

A Li-Li nn-pair is an axial center with a strong local polarization field. Because the energy required to reorient an Li-Li nn-pair axis by 90° is large, 1432 K, PNC polar orientations resist coarsening that involves reorientation(s) of Li-Li nn-pair axes. This constraint on FE-percolation[7] may explain the observation of a dipole-glass like state in the $0 < x < 0.02$ concentration range[3,5].

The average distance between Li-Li nn-pairs is obviously larger than the average distance between isolated Li-ions because the concentration of Li-Li nn-pairs (x_{Li-Li}) is so much lower ($x_{Li-Li} \approx 3x_{Li}^2$ for small x). Therefore, it is plausible to think in terms of randomly oriented but interacting PNC that each contain one Li-Li nn-pair as the "seed" plus several isolated Li-ions. Such a system has an interesting phase diagram.[15]

If one excludes strains from a mean field Hamiltonian then there are two variables: one for a soft-mode; the other for Li-dipoles. Both contribute to the dielectric response, but the former is essentially dispersionless far below the soft-mode frequency. The Li-dipole term however has relaxational character. Neglecting the damping of Li-oscillations within Li wells, but accounting for jumps between nn Li-wells, Li-dipole associated with z-polarization of an isolated Li-ion in a cubic environment is:

$$D_z = n\mu\,(w_z - w_{-z}) \quad (12)$$

where μ is the magnitude of the Li-dipole. Only one relaxation process (of T_{1u} symmetry) contributes to polarization fluctuations, and the polarization takes the form[46]

$$D_z = n\mu^2 F(T)\tilde{E}_z \quad (13)$$

where

$$F(T) = \frac{1}{6k_BT}\frac{1}{4k+i\omega} \quad (14)$$

Here $\tilde{E}_z = E_z + \lambda P_{TO}$ is the local field, λ a coupling constant, E_z an external field, P_{TO} the polarization connected with the soft-mode, and $\tau = 4k$ the relaxation time for the T_{1u} relaxation process. The dielectric susceptibility connected with Li jumps can be written as

$$\chi_{Li} = \frac{1}{\varepsilon_0}\frac{dD_z}{dE_z} = \frac{n\mu^2}{\varepsilon_0}F(T)\,(1+\lambda\varepsilon_0\chi_{TO}) \quad (15)$$

where

$$\chi_{TO} = \frac{dP_{TOz}}{\varepsilon_0 dE_z} \quad (16)$$

This derivative can be found from a Landau expansion after excluding strains (Sec. III G)

$$\chi_{TO} = \frac{1}{\varepsilon_0 A(T)}\,(1+\lambda\varepsilon_0\chi_{Li}) \quad (17)$$

where

$$A(T) = \alpha + 3\beta P_{TO}^2 + 5\gamma P_{TO}^4 \quad (18)$$

Here the nonlinearity coefficient β is already renormalized after the elimination of strains. One obtains

$$\chi = \chi_{TO} + \chi_{Li} = \\ = \frac{1}{\varepsilon_0}\frac{1+4\lambda n\mu F(T)+4\mu^2 nA(T)F(T)}{A(T)-\lambda^2 nF(T)} \quad (19)$$

This result is consistent with earlier work[4]: the dielectric susceptibilities of the host structure and Li-dipoles are both enhanced by mutual coupling; T_c increases and frequency dispersion is enhanced.

There are two relaxation processes in KLT. Mathematically this only changes F(T) by adding a contribution with the rate $k_{bc}k_{ab}/k_{ba}$ for Li-Li nn-pairs. Frequency dispersion is dominated by two relaxation processes, 90° and 180° (compare this approach with experimental results in Refs.[12,47]).

The relaxational part of the susceptibility can be described by kinetic equations for the occupation probabilities for different potential wells around Li-occupied A-sites. This procedure can be applied to any PNC if one knows the kinetic coefficients. The temperature dependence of these coefficients is common, and it is mainly controlled by the barrier height U which can be computed from FP; the temperature dependence of the relaxation time is

$$\begin{aligned}\tau &= A\chi(T)\int_{-\infty}^{\infty} e^{\left(U+ay^2\right)/k_BT}dy = \\ &= A\chi(T)\sqrt{\frac{\pi k_BT}{a}}e^{U(T)/k_BT} = \\ &= \tau_0\left(T\right)e^{U(T)/k_BT} \end{aligned} \quad (20)$$

which accounts for Li-jumps over [110]-type saddle points; χ is the dielectric permittivity of the media in which the Li-dipoles are embedded; a is a constant determined by the spring constant at the saddle point.

V. CONCLUSIONS

Calculations on a 40-atom KLT supercell that contains one Li-ion (KLT40) indicate that there is only one instability connected with Li off-centering. This instability is associated with large Li-displacement in the [001] direction, relative to an ideal A-site position. Li potential wells are separated by potential barriers with [110]-type saddles. Calculated [110] potential barriers and [0,0,d] Li-displacements, in fully relaxed KLT, are in good agreement with values obtained by fitting a mean field expansion to experimental data[11,12].

All ions in the KLT40 supercell are displaced from their ideal positions but the O-ions closest to Li exhibit the largest sympathetic displacements; in the opposite direction as Li, and closer to one another. Calculated vibrational frequencies for fully relaxed KLT40 indicate that A_1- and E-symmetry modes originate from the TO soft-mode. The energy of the center of gravity for these states is higher than the T_{1u} state in pure KT, which indicates that the addition of Li-ions hardens the TO soft-mode.

The A_1- and E-modes have an admixture of Li-vibrations, at about 300 cm^{-1}. The TO soft-mode and orientational Li-polarization are coupled.

Berry phase analyses yielded total dipole moments associated with Li off-centering that are ∼5 times larger than the Li-dipole moment itself. This enhancement is primarily caused by O-relaxation around the off-centered Li-ion.

In a tetragonally distorted KLT40 supercell (in tension) the minimum-energy orientation for a Li-dipole is along the c-axis. The equilibrium state of uniformly polarized KLT is slightly tetragonal; conversely, tetragonal distortion of KLT enhances polarization.

First-principle calculations of Li-Li nn-pair excitations in a KLT80 supercell strongly support the conclusion of Dousenau et al.[10] that the 180° relaxation process is caused by $z - z \rightleftharpoons \overline{z} - \overline{z}$ Li-Li nn-pair flipping.

ACKNOWLEDGMENT

We thank G. Kresse for providing an LDA pseudopotential for Ta. S.A.P. thanks NIST for hospitality and RFBR grant No. 01-02-16029.

REFERENCES

[1] G.A. Samara, B. Morosin. Phys. Rev. B **8**, 1256 (1973).
[2] J. J. van der Klink and F. Borsa, Phys. Rev. B **30**, 52 (1984).
[3] U. T. Höchli, K. Knorr and A. Loidl, Adv. Phys. **39**, 405 (1990).
[4] B. E. Vugmeister and M. D. Glinchuk, Rev. Mod. Phys. **62**, 993 (1990).
[5] W. Kleemann, V. Shönknecht, D. Sommer, and D. Rytz, Phys. Rev. Lett. **66**, 762 (1991).
[6] P. Voigt and S. Kapphan, J. Phys. Chem. Sol. 55, 853 (1994).
[7] S. A. Prosandeev, V. S. Vikhnin, S. Kapphan, Eur. Phys. J. B **15**, 469 2000.
[8] H. M. Christen, U. T. Höchli, A. Chatelain, and S. Ziolkiewicz, J. Phys.: Condens. Matter 3, 8387 (1991).
[9] P. Doussineau, T. de Lacerda-Arôso and A. Levelut, J. Phys.: Condens. Matter **12**, 1461 (2000).
[10] P. Doussineau, Y. Farssi, C. Frenos, A. Levelut, K. McEnaneu, J. Toulouse, S. Ziolkiewicz, Europhys. Lett. **24**, 415 (1993).
[11] R. K. Pattnaik, J. Toulouse, and B. George, Phys. Rev. B **62**, 12820 (2000).
[12] S. A. Prosandeev, V. A. Trepakov, M. E. Savinov, L. Jastrabik, and S. E. Kapphan, J. Phys.: Condens. Matter **13**, 9749 (2001).
[13] U. T. Höchli, J. Hessinger, and K. Knorr, J. Phys.: Condens. Matter 3, 8377 (1991).
[14] P. M. Gehring, S. Wakimoto, Z.-G. Ye, and G. Shirane, Phys. Rev. Lett., **87**, 277601-1 (2001).
[15] A. E. Maslennikov, S. A. Prosandeev, V. S. Vikhnin, S. Kapphan, Integr. Ferroelectrics **38**, 797 (2001).
[16] H. Vollmayr, R. Kree, and A. Zippelius, Phys.Rev. B **44**, 2 (1991).

[17] M. P. Ivliev and V. P. Sakhnenko, Fiz. Tverd. Tela **28**, 632 (1986).
[18] M. Exner, C. R. A. Catlow, H. Donnerberg and O. F. Schirmer, J. Phys.: Condens. Matter **6**, 3379 (1994).
[19] R. I. Eglitis, A. V. Postnikov and G. Borstel, Phys. Rev. B **55**, 12976 (1997).
[20] I. I. Tupitsin, A. Deineka, V. A. Trepakov, L. Jastrabik and S. E. Kapphan, Phys. Rev. B **64** 195111 (2001).
[21] A. V. Postnikov, T. Neumann and G. Borstel, Ferroelectrics **164**, 101 (1995).
[22] R. S. Klein, G. E. Kugel, M. D. Glinchuk, R. O. Kuzan, I. V. Kondakova, Phys .Rev. B. 50 (1994 II) 9721- 9728; V. V. Laguta, M. D. Glinchuk, I. P. Bykov, J. Rosa, L. Jastrabik, R. S. Klein and G. E. Kugel, Phys. Rev. B **52**, 7102 (1995).
[23] P. Sangalli, E. Giulotto, L. Rollandi, P. Calvi, P. Camagni, and G. Samoggia, Phys. Rev. B **57**, 6231 (1998).
[24] P. Galinetto, E. Giulotto, P. Sangalli, P. Camagni and G. Samoggia, J. Phys.: Condens. Matter **11**, 9045 (1999).
[25] G. Kresse and J. Hafner, Phys. Rev. B **47**, 558 (1993).
[26] G. Kresse and J. Furthmüller, Phys. Rev. B **54**, 11169 (1996).
[27] D. Vanderbilt, Phys. Rev. B **41**, 7892 (1990).
[28] G. Shirane, R. Newnham, and R. Pepinsky, Phys. Rev. **96**, 581 (1954).
[29] D. J. Singh, Ferroelectrics **164**, 143 (1991).
[30] Because of weak coupling with another mode with similar frequency, the 205 cm^{-1} mode of pure KT actually is split into 200 cm^{-1} and 205 cm^{-1} modes of KLT40.
[31] I. Inbar and R. Cohen Ferroelectrics **194**, 83 (1997).
[32] G. Yong, J. Toulouse, R. Erwin, S. M. Shapiro and B. Hennion, Phys. Rev. B **62**, 14736 (2000).
[33] H. Vogt, J. Phys.: Condens. Matter **7**, 5913 (1995).
[34] J. J. Van der Klink and S. N. Khana, Phys. Rev. B **29**, 2415 (1984).
[35] J. Toulouse, B. E. Vugmeister and R. Pattnaik, Phys. Rev. Lett., 73, 3467 (1994).
[36] C. -C. Su, B. Vugmeister, and A. G. Khachaturyan, J. Appl. Phys. **90**, 6345 (2001).
[37] J. D. Axe, Phys. Rev. **157**, 429 (1967).
[38] M. Stachiotti, R. Migoni, J. Kohanoff and U. T. Höchli, Ferroelectrics **157**, 335 (1994).
[39] M. G. Stachiotti and R. L. Migoni, J. Phys.: Condens. Matter **2**, 4341 (1990); M.G. Stachiotti, R. L. Migoni, and U. T. Höchli, J. Phys.: Condens. Matter **3**, 3689 (1991).
[40] R. K. Pattnaik and J. Toulouse, Phys. Rev. B **60**, 7091 (1999).
[41] W. Zhong, D. Vanderbilt,, and K.M. Rabe, Phys. Rev. B **52**, 6301 (1995).
[42] U. V. Waghmare, K. M. Rabe, H. Krakauer, R. Yu, and C.-Z. Wang, in *First Principle Calculations for Ferroelectrics* (AIP Conference Proceedings 436), edited by R.E. Cohen, AIP, Woodbury, NY (1998), p. 32.
[43] K. M. Rabe and U. V. Waghmare, Phys. Rev. B **52**, 13236 (1995).
[44] U. V. Waghmare and K. M. Rabe, Phys. Rev. B **55**, 6161 (1997).
[45] S. A. Prosandeev, V. S. Vikhnin and S. E. Kapphan, J. Phys.: Condens. Matter **14**, 4407 (2002).
[46] S. A. Prosandeev, Phys. Sol. St. **43**, 1948 (2001).
[47] S. A. Prosandeev and V. A. Trepakov, J. Exp. Theor. Phys. **94** 419 (2002).